# FATIGUE CRACK PROPAGATION IN RAILWAY AXLES

V. Gros*, C. Prioul*, Ph. Bompard* and P. Lallet**

Fatigue crack growth has been studied in a medium carbon normalised steel using tension-compression tests for different stress ratios. The evolution of $K_{op}$, determined by CTOD measurements for R=0, reveals that $K_{op}/K_{max}$ decreases as $K_{max}$ increases. This study shows that, by using appropriate models it is possible, for $R > 0$, to plot all the experimental results on a unique line on the da/dN versus $\Delta K_{eff}$ diagram. Classically, the effect of the compressive part of the fatigue cycle on $K_{op}$ is not taken into account by these models. Nevertheless, the tension-compression fatigue tests show that, for the same $\sigma_{max}$ value, crack growth rate increases as the stress ratio goes from zero to a negative value. A modified version of Newman's model is proposed in order to account for these observations.

## INTRODUCTION

The railway axle is one of the main security parts of trains. It is made of normalised medium carbon steel, and subjected to cyclic rotary bending. Fatigue is a potential cause for axle fracture. Fatigue cracks, which are usually initiated at notches resulting from the impact of ballast on the axle body, are found during periodic testing using non destructive methods. Therefore, in order to adapt the survey periodicity of the axle to new service conditions, it is of great importance to accurately evaluate the axle residual fatigue life, after crack initiation.

The diameter of the axle is large enough to suppose that the stress gradient is very small compared to the dimension of the notch on the surface and therefore it is possible to replace bending by tension. Subsequently, the fatigue crack growth has been studied using tension tests on compact tension specimens (CT) and tension-

* Ecole Centrale de Paris, Laboratoire MSS/MAT, CNRS URA 850, Grande Voie des Vignes, 92295, Châtenay Malabry, France.
** SNCF, Direction du Matériel et de la Traction, Division des Laboratoires, 6 place du 8 mai 1945, 92300, Levallois-Perret, France.

compression tests on center cracked tension specimens (CCT). The evolution of the cracks during the propagation stage, has been investigated by successive observation of the specimen's surface and measurement of the different crack lengths. These observations allow to determine the crack growth rate for the different stress ratios and to plot the corresponding Paris law. In order to specify the different growth rates, we'll use the effective stress intensity factor $K_{eff}$ using the $K_{opening}$ factor introduced by Elber. Many authors have shown that a crack propagates only when it is opened. Some of them have noted the detrimental effect of the compressive parts of the cycles on the fatigue growth rate.

## MATERIAL AND EXPERIMENTAL PROCEDURE

The material tested is a normalised medium carbon steel in the form either of rolled bars about 65 mm in diameter, or of railway axles. The chemical composition (wt. %) is reported in Table 1. The microstructure is ferrito-pearlitic with lamellar pearlite and the mean grain size is about 20 μm.

TABLE 1 - Chemical composition (Weight %) of the medium carbon steel.

| C | Mn | Cr | Ni | Ti | Cu | Si | P | S |
|---|---|---|---|---|---|---|---|---|
| 0,41 | 0,76 | 0,09 | 0,08 | 0,01 | 0,19 | 0,23 | 0,01 | 0,02 |

The mechanical properties (yield stress $\sigma_y$, ultimate tensile strength $\sigma_u$, fatigue limit $\sigma_w$) are reported in Table 2.

TABLE 2 - Mechanical properties of the normalised medium carbon steel.

| $\sigma_{ys}$ (MPa) | $\sigma_u$ (MPa) | $\sigma_w$ (MPa) | A % |
|---|---|---|---|
| 350 | 600 | 270 | 25 |

The CCT specimens were machined from the bars after a 160 minute normalising heat treatment at 860°C. The CT25 specimens were machined directly from the railway axles which have the same properties as the bars.
Fatigue tests were undertaken at a frequency of 30 Hz on a Schenck servo-hydraulic machine. The observations of the crack propagation were realized with a binocular microscope placed in front of the specimens. The accuracy of these measurements is about 50 μm. The measurements of $K_{op}$ were conducted by crack mouth opening displacement (CMOD).

## RESULTS AND DISCUSSION

In figure 1 the evolution of the crack growth rate has been plotted versus the maximum stress intensity factors for different stress ratios, varying from 0.7 to -1. The results for positive stress ratios were obtained on CT specimens, whereas the results for R =-1 were obtained on CCT ones. As expected, the data are not aligned on a single Paris curve, due to the influence of the crack closure effect. Therefore, in order to introduce the effective stress intensity factor, the crack opening stress intensity factor ($K_{op}$) was measured by the CMOD method applied on CT

specimens, with stress ratios close to zero. The evolution depicted in figure 2, indicates that $K_{op}$ remains nearly constant for small values of $K_{max}$ and then increases for larger values of $K_{max}$. Plotting the same results, but with $K_{op}$ normalised by $K_{max}$, produces a monotonously decreasing curve (already reviewed by McClung) which has been fitted to the analytical expression :

$$\frac{K_{op}}{K_{max}} = \frac{0,1K_{max} + 2,77}{K_{max} - 2,63}$$

This expression can be used to calculate the effective stress intensity factor ($K_{eff}$) for positive stress ratios only, and to plot the modified Paris diagram in terms of $K_{eff}$. This diagram (curves not reported) shows that, by using this procedure, and by considering that the data obtained at R = -1 can be treated as data obtained at R = 0, a master Paris curve represents quite well all the data for positive stress ratios, but the data obtained at a negative R ratio (R=-1) do not fit this master curve. Therefore, a reverse method was applied to determine the appropriate $K_{op}$ value to be applied to a negative R ratio data in order to gather the whole set of data (negative and positive stress ratio) on a single master Paris curve plotted in terms of $K_{eff}$ (figure 3).

The normalised $K_{op}$ values used to obtain this unique Paris plot, whatever the stress ratio, are represented in figure 4, as a function of $K_{max}$. The values at R = 0 are those obtained from the experiments and figure 2's analytical fitting. $K_{op}$ values at R = -1 are deduced from the reverse method mentioned above. This figure 4 corresponds to a modified Newman's diagram in which the maximum cyclic stress ($\sigma_{max}$) has been replaced by the maximum cyclic stress intensity factor ($K_{max}$), in order to allow the representation on the same diagram of results obtained by both CT and CCT tests.

In the Newman model, the data for $K_{op}$ are linearly interpolated for negative stress ratios, and by a cubic polynomial expression for positive stress ratios. A similar interpolation method has been used to construct figure 4, $\sigma_{max}/\sigma_o$ being replaced by $K_{max}$ as described above :

$$K_{eff} = K_{max} - K_{op}$$

with $$\frac{K_{op}}{K_{max}} = A_0 + A_1 R \qquad \text{for} \quad -1 \le R < 0$$

and $$\frac{K_{op}}{K_{max}} = A_0 + A_1 R + A_2 R^2 + A_3 R^3 \qquad \text{for} \quad R \ge 0$$

The parameters $A_0$ and $A_1$ are determined experimentally : $A_0$ is deduced from the $K_{op}$ values plotted in figure 2 versus $K_{max}$, and $A_1$ is adjusted in order to have the best fit for the entire set of data in the Paris plot (fig. 4).

The parameters $A_2$ and $A_3$ are calculated in order to fulfil both the equation $K_{op} = K_{max}$ for R = 1 whatever $K_{max}$, and the condition of having, for R = 1, a tangent with a slope varying from zero for $K_{max}$ near $K_{threshold}$ to 1 for the curves with high values of $K_{max}$.

These conditions can be summarised as follows :

$$\text{if} \quad K_{op} \geq K_{min} \left\{ \begin{array}{c} A_0 = f(K_{max}) \\ A_1 = \alpha \cdot K_{max} \\ A_2 = 1 - A_0 - A_1 - A_3 \\ A_3 = 2A_0 + A_1 - 1 - \exp(K_{th} - K_{max}) \end{array} \right\}$$

and $\quad \text{if} \quad K_{op} < K_{min} \quad \text{then} \quad K_{eff} = K_{max} - K_{min} = (1-R)K_{max}$

From the modified Newman's diagram plotted in figure 5, the detrimental effect of the compressive part of cyclic loading of the steel studied is clearly put into evidence. This effect is characterised mainly by the positive slope of the straight line describing the evolution of the opening stress intensity factor versus stress ratio, for negative stress ratios. Furthermore, even negative opening stress intensity factors can be obtained for high compressive stresses, which could correspond to positive residual stress after compressive loading.

This effect is confirmed by fatigue tension compression tests performed in order to simulate the variable stress amplitude cycles corresponding to real service conditions of railway axles. Two cases were considered. In the first test, complete cycles at R = -1 are applied on the specimen, whereas in the second test, the compressive part of the signal is replaced by a zero applied stress. The comparison of the results of these two different experimental procedures reveals that the number of cycles to failure is three times higher for variable amplitude tests at R = 0 than for similar tests at R = -1 (fig. 6).

Furthermore, if a constant stress amplitude test at R = -1 is interrupted and changed to a constant stress amplitude test at R = 0, with the same maximum cyclic stress, a temporary crack arrest is noted and crack arrest lines can be observed on the surface of the crack.

Usually, a complete experimental simulation of service conditions is not possible due to the large number of cycles applied. Therefore the tests are generally accelerated by considering that low amplitude cycles, close to the threshold stress intensity factor, do not contribute to crack growth. Nevertheless, by assuming this, fatigue life predictions, derived from crack propagation models based on $K_{eff}$, lead to longer fatigue life, as compared with real fatigue life measurements. A parametric study of these models also shows that they are extremely sensitive to the experimental determination of the m and C parameters of the Paris law, as well as to the values of the threshold stress intensity factor ($K_{th}$) and the opening stress intensity factor ($K_{op}$) which are introduced in the model.

The inadequacy of these models can be attributed to the influence of low cyclic stress cycles, which are much more numerous, and finally play an important cumulative part in contributing to crack propagation, especially if negative stress ratios are applied.

In medium carbon steels this detrimental effect of the compressive part of fatigue cycles could be attributed to the tensile residual stresses developed in the crack wake by the compressive stresses. Both cinematic hardening and the Bauschinger effect certainly play an important role in the development of these tensile residual stresses. We are now modeling these effects by FEM and a release node technique.

## CONCLUSIONS

A realistic prediction of residual service life through the evaluation of crack propagation in a medium carbon steel from notches must :

- incorporate the effects of the compressive part of fatigue cycles, as these have been found to accelerate the crack propagation rate,
- include a significant number of cycles at low stress level.

## REFERENCES

(1) Elber, W., "Fatigue crack closure under cyclic tension", Engineering Fracture Mechanics, Vol.2, 1970,.pp. 37-45.

(2) Newman, J. C., "A crack opening stress equation for fatigue crack growth", International Journal of Fracture, Vol. 24, 1984, pp. R131-R135.

(3) McClung, R.C., "The influence of applied stress, crack length, and stress intensity factor on crack closure", Metallurgical Transactions A, Vol.22A, july 1991, pp. 1559-1571.

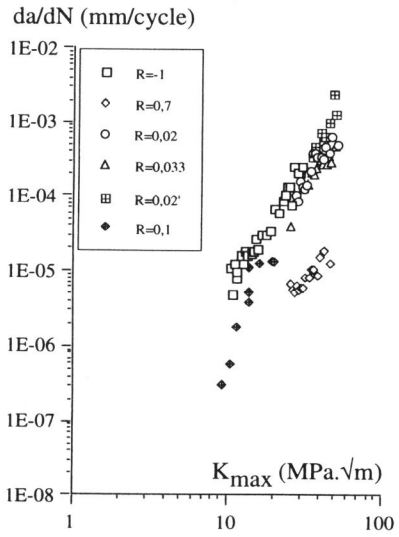


Figure 1 : Experimental crack growth rates for different stress ratios

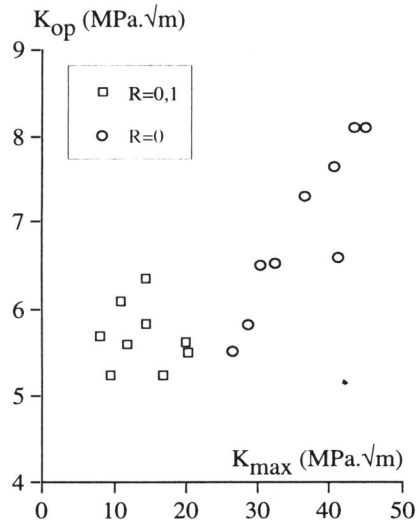


Figure 2 : Experimental $K_{op}$ versus $K_{max}$ for R ratio close to zero

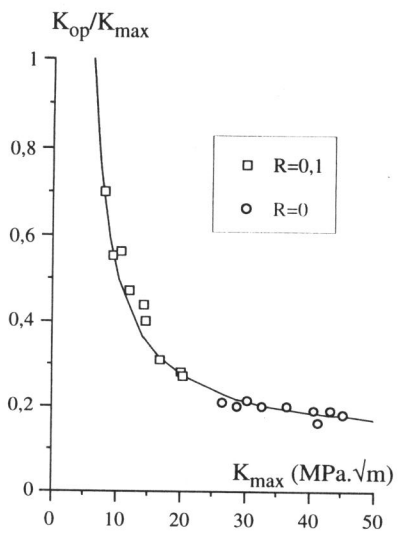


Figure 3 : Evolution of the normalised $K_{op}/K_{max}$ versus $K_{max}$

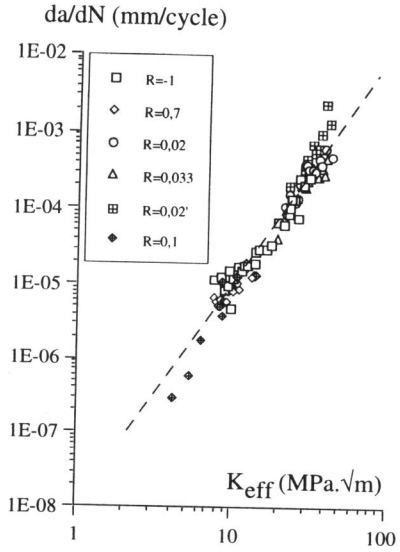


Figure 4 : Crack growth rates versus $K_{eff}$ with the model presented

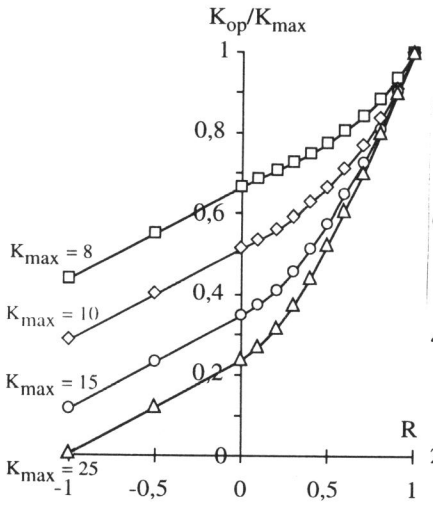


Figure 5 : Modified Newman's model

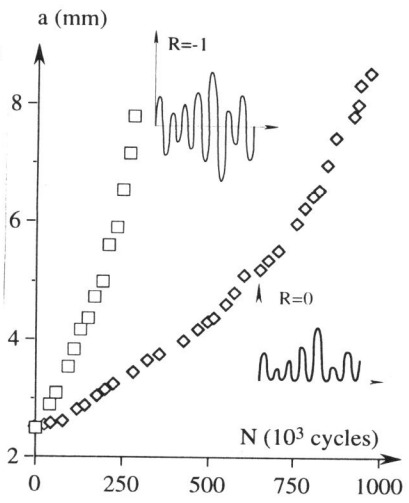


Figure 6 : Experimental effect of compressive parts of cycles on crack evolution